Stabilized and Modified Mixed *u/p* Finite Element Formulation for Incompressible Elastic Media using Equal-Order Triangular Elements

Giancarlo P. Ventura* and Mark Albert H. Zarco
Institute of Civil Engineering, College of Engineering,
University of the Philippines Diliman, Quezon City, Philippines
*Corresponding author: gpventura@up.edu.ph

Abstract – *The finite element method is a powerful computational technique used to solve complex problems. However, the method encounters limitations when dealing with incompressible media represented by a Poisson's ratio equal to 0.5. Because of this, mesh locking occurs as certain elements of matrices blow up as others disappear due to the nature of incompressible elasticity that leads to stress oscillations and inaccurate deformation behaviors. This study addresses these challenges by developing a stabilized and modified mixed formulation utilizing equal-order triangular elements. The proposed modified mixed formulation incorporates both displacements and pressures as degrees of freedom by treating them independently, and decoupling stresses and strains by decomposing them into their volumetric and deviatoric parts. Furthermore, the Beltrami-Michell equations are incorporated as a set of compatibility equations to close the boundary value problem. A stabilizing term based on Galerkin mixed methods is introduced to maintain the well-posedness of the problem, addressing issues such as ill-conditioning of the stiffness matrix and preventing spurious stresses. The study also emphasizes the efficiency of unstructured lower order triangular meshes, which, when stabilized, offer a balance between computational cost and accuracy. Since there is limited to no literature regarding the application of such methods in an axisymmetric case, a representative problem in the form of an infinite half-space loaded by a circular footing is presented and validated to demonstrate the effectiveness of the proposed method. The example highlights the formulation's ability to provide accurate results, validating its robustness and practical applicability in various engineering scenarios.*

Keywords: finite element method, incompressible elasticity, mixed formulation, triangular elements

I. INTRODUCTION

Modeling physical phenomena enables the understanding of a wide array of natural and engineered systems. Almost every single phenomenon in nature can be rigorously described using scientific law and mathematical principles. These descriptions often take the form of algebraic, differential, or integral equations that relate various quantities characterizing the phenomena [1]. Practical applications of such modeling in the field of civil engineering are vast and diverse – they include determining stress distributions in bridges and dams, analyzing soil stability for foundation design, and simulating groundwater flow to predict contaminant transport among others. Each of these examples underscores the critical role of accurate mathematical modeling in solving complex real-world problems and advancing engineering knowledge.

With the ever-advancing capabilities of computers, computational mechanics has been front and center in the development of mathematical models using numerical methods to solve various physical phenomena. One powerful computational tool for addressing these complex problems is the finite element method (FEM). It is a numerical technique for finding approximate solutions to boundary value problems for partial differential equations. By breaking down a large system into smaller, simpler parts called finite elements, the method provides a framework for constructing a solution through the assembly of these simpler elements. It is particularly advantageous in handling problems with irregular geometries, complex boundary conditions, and material heterogeneities. The versatility and robustness of the finite element method have made it a cornerstone in the toolkit of anyone engaged in modeling and simulation.

While the finite element method is generally reliable for solving most types of problems, it encounters limitations when applied to incompressible or nearly incompressible systems. Many materials of significant importance involve motions that essentially preserve local volumes. This means that after deformation, each small portion comprising the medium retains the same volume as before. Imposing incompressibility conditions results in mesh locking, where the model fails to deform properly in certain directions under the applied loading conditions. The displacement response of the model is poor because the elements lock due to volume preserving constraints. Incompressibility also leads to other numerical issues, such as the ill-conditioning of the stiffness matrix and large stress oscillations at the numerical integration points [2].

Mesh locking has been addressed through the introduction of stabilizing methods [3], though most of these methods have been developed for higher-order meshes. Higher-order meshes are preferred for their improved accuracy compared to lower-order meshes. However, lower-order meshes offer significant advantages as well. In finite element analysis, mesh generation and element integration are typically the most time-consuming tasks. Lower-order unstructured meshes simplify these processes, resulting in faster calculations. Additionally, unstructured low-order meshes are more user-friendly for inexperienced users, as they require fewer inputs and reduce concerns about the meshing procedure. Also, they offer lower computational costs which would be ideal for efficient time and memory allocation in computational programs.

The standard formulation used for the finite element solution is the displacement-based method, which is widely used, efficient, and effective except for incompressible materials. Due to incompressibility, a basic observation in the analysis is that the pressure is difficult to predict accurately [4]. Because of these reasons, a modified mixed displacement (u) – pressure (p) formulation which interpolates both displacements and pressures is a more suitable approach in the analysis of incompressible materials. Furthermore, stable and accurate mixed u/p formulations in incompressible materials are required to satisfy the Ladyzenskaya–Babuška–Brezzi (LBB) condition [5,6], also known as the inf-sup condition which ensures that the solution of a saddle point problem exists, is unique, and is well-posed. However, for equal-order linear interpolation, which is the most convenient combination for practical purposes, the LBB condition is not satisfied [7]. Equal order interpolation refers to the use of the same polynomial degree to interpolate both the displacement field and the pressure field within the

elements of the finite element mesh. Despite being computationally convenient, using the same interpolation space for both displacement and pressure fields does not allow enough degrees of freedom to satisfy the incompressibility constraint.

To overcome all the issues discussed, this present work formulates a stabilized mixed u/p formulation for unstructured equal-order triangular finite elements which can be used for incompressible materials. The stabilization technique is based on Galerkin mixed methods [7–10] to improve the performance of the linear triangle.

II. THEORETICAL FORMULATION

The following section will introduce the proposed stabilized modified mixed formulation for incompressible materials, highlighting its significance and applications in addressing the challenges associated with modeling incompressible materials.

Traditional u/p formulations and stabilization techniques [11-17] while effective in some cases, the underlying reasons for the success of the techniques remain unclear. The finite element approximations in previous studies require independent interpolations for both displacements and pressures and should satisfy the LBB condition. The present work improves upon these traditional techniques by offering a more mathematically sound approach grounded on well-established principles. While the key differences are discussed throughout this section as the formulation details are presented, two major points distinguish this study: (1) The decomposition of the stress components is different. The traditional stabilization techniques are based on a stress decomposition in which p is only equal to the mean stress for the case of incompressible elasticity, whereas in this study, the formulation involves a true volumetric-deviatoric decomposition in which p is equal to the mean stress regardless of the value of the Poisson's ratio, and (2) In traditional stabilization techniques, the basis for adding the Laplacian of pressure is not clear and appears to be arbitrary, often justified only by its empirical success (i.e. included just because it seems to work). In the presented formulation, however, the Laplacian of p is included to enforce the condition that p must satisfy the Beltrami-Michell equations.

2.1 Pure displacement-based formulation

Consider the domain Ω of an isotropic material with a Young's modulus E and a Poisson's ratio ν that is bounded by $\Gamma = \Gamma_u \cup \Gamma_t$ and $\Gamma_u \cap \Gamma_t = \emptyset$. From the balance of linear momentum, the strong form of the boundary value problem can be stated as

Given $f: \Omega \to R, \bar{u}: \Gamma_g \to R, \bar{t}: \Gamma_h \to R$, find $u: \overline{\Omega} \to R$ such that

$$\nabla \cdot \sigma + f = 0 \ \text{in} \ \Omega \tag{1}$$

$$u = \bar{u} \ \text{on} \ \Gamma_u \tag{2}$$

$$\sigma \cdot n = \bar{t} \ \text{on} \ \Gamma_t \tag{3}$$

To complete the boundary value problem, a constitutive equation is needed to describe the relationship between stresses and strains. In linear elasticity, Hooke's law states that

$$\sigma = \mathbb{C} : \varepsilon \tag{4}$$

where the fourth order elasticity tensor has the following components

$$C_{ijkl} = \lambda \delta_{ij} \delta_{kl} + \mu (\delta_{ik} \delta_{jl} + \delta_{il} \delta_{jk}) \tag{5}$$

Note that λ and μ are the Lamé parameters which can be related to E and ν through the following equations

$$\lambda = \frac{\nu E}{(1 + \nu)(1 - 2\nu)} \tag{6}$$

$$\mu = \frac{E}{2(1 + \nu)} \tag{7}$$

Similarly, the bulk modulus K is defined as

$$K = \frac{E}{3(1 - 2\nu)} \tag{8}$$

As ν approaches 0.5 the resistance to volume change assuming a constant resistance to shearing increases greatly [18], as shown by the ratio of the bulk modulus to the shear modulus

$$\frac{K}{\mu} = \frac{2(1 + \nu)}{3(1 - 2\nu)} \tag{9}$$

Notice that the ratio approaches infinity as ν approaches 0.5. The limiting value, $\nu = 0.5$ represents incompressibility and creates problems in the constitutive relationships of elasticity. The constitutive equations are written as

$$\sigma = \lambda \mathrm{tr}(\varepsilon) 1 + 2\mu\varepsilon \tag{10}$$

where 1 is the identity dyadic. The Lamé parameter λ can be written as

$$\lambda = \frac{2\nu\mu}{1 - 2\nu} \tag{11}$$

It is clear that λ will also be unbounded when the material is incompressible.

The effectiveness of the displacement-based formulation lies in its conceptual simplicity. By applying the principle of virtual work, a set of simultaneous equations with nodal point displacements as unknowns is generated. These displacements can then be used to calculate stresses and strains. However, this method has several undesirable characteristics, including

the ill-conditioning of the stiffness matrix, spurious or incorrect stresses (particularly pressures), and locking (a loss of accuracy in the computed response as incompressibility is enforced) [19, 20] which are consequences of the relationships shown earlier. Hence, another approach should be used.

2.2 Decomposition of stresses and strains

Since the pressure is difficult to predict in incompressible media, it is favorable to have a formulation which decouples it from the displacements. The Cauchy stress tensor σ can be additively decomposed into a scalar volumetric component p, and a dyadic deviatoric component s as follows

$$\sigma = p1 + s \tag{12}$$

and the deviatoric component satisfies the condition

$$s : 1 = 0 \tag{13}$$

It can be shown that the volumetric component p is given by

$$p = \frac{1}{3}(\sigma : 1) \tag{14}$$

and the deviatoric component s is given by

$$s = \sigma - p1 = A : \sigma \tag{15}$$

such that

$$A = I - \frac{1}{3}(1 \otimes 1) \tag{16}$$

and I is the is the 4th order identity tensor.

Similarly, the infinitesimal small strain tensor ε is given by

$$\varepsilon = \frac{1}{2}[\nabla u + (\nabla u)^T] \tag{17}$$

where u is the displacement field vector. The strain tensor can be further decomposed into a scalar volumetric component ε_v and a dyadic deviatoric component ε_d as follows

$$\varepsilon = \varepsilon_v 1 + \varepsilon_d \tag{18}$$

where the deviatoric component satisfies the condition

$$\varepsilon_d : 1 = 0 \tag{19}$$

It can be shown that the volumetric component ε_v is given by

$$\varepsilon_v = \varepsilon : 1 = \nabla \cdot u \tag{20}$$

while the deviatoric component ε_d is given by

$$\varepsilon_d = \varepsilon - \frac{1}{3}\varepsilon_v 1 = \frac{1}{2}[\nabla u + (\nabla u)^T] + \frac{1}{3}(\nabla \cdot u)1 = A : \frac{1}{2}[\nabla u + (\nabla u)^T] \tag{21}$$

Furthermore, the constitutive relationship between the stress σ and the strain $\boldsymbol{\varepsilon}$ based on the Generalized Hooke's Law can be written separately for the volumetric and deviatoric components as

$$p = K\varepsilon_v \tag{22}$$

$$s = 2\mu\varepsilon_d \tag{23}$$

where μ is the shear modulus. Notice as well that the decomposition of the strains leads to a decoupled expression of the stress tensor as well. The preceding constitutive relationships are valid for compressible elasticity. With decreasing compressibility, $K \to \infty$, and consequently

$$\varepsilon_v = \nabla \cdot u = \frac{p}{K} \to 0 \tag{24}$$

2.3 Beltrami-Michell equations

The Beltrami-Michell equations [21-23] are a set of six partial differential equations which are written completely in terms of the Cauchy stress σ. They form an alternative set of governing differential equations for an elastostatic boundary value problem and is expressed as

$$\nabla^2 \sigma + \left(\frac{1}{1+\nu}\right)\nabla\nabla\theta + [\nabla f + (\nabla f)^T] + \left(\frac{\nu}{1-\nu}\right)(\nabla \cdot f)1 = 0 \tag{25}$$

where $\theta = \sigma : 1 = 3p$, ν is the Poisson's ratio, and f is the body force per unit volume vector.

It can be shown that the Beltrami-Michell equations involving the normal stress components can be combined into a single equation in terms of θ

$$\nabla^2\theta = 3\nabla^2 p = -\left(\frac{1+\nu}{1-\nu}\right)\nabla \cdot f \tag{26}$$

For the case of incompressible elasticity in which $\nu = 0.5$, the above equation reduces to

$$\nabla^2 p + \nabla \cdot f = 0 \tag{27}$$

For the case where f is constant through the problem domain such that $\nabla \cdot f = 0$, the

following equation results for both compressible and incompressible elasticity

$$\nabla^2 p = 0 \tag{28}$$

The Beltrami-Michell equations provide the necessary and sufficient conditions for an equilibrated stress field to be compatible with the displacement field in the body [24].

2.4 Strong form of the problem

Given the problem domain Ω bounded by Γ, the boundary value problem involves finding the displacement u and mean stress p that satisfy pointwise the following differential equations.

Imposition of the conservation of linear momentum results in the following equation

$$\nabla \cdot \sigma + f = 2\mu\nabla \cdot \varepsilon_d + \nabla p + f = 0 \tag{29}$$

The volumetric component of the Generalized Hooke's Law results in the equation

$$\nabla \cdot u - \frac{p}{K} = 0 \tag{30}$$

For the case of incompressible elasticity, the preceding equation simplifies to

$$\nabla \cdot u = 0 \tag{31}$$

From the Beltrami-Michell equation, the following equation results assuming constant body forces within the problem domain

$$\nabla^2 p = 0 \tag{32}$$

subject to the boundary conditions: $u = \bar{u}$ on Γ_u and $t = \sigma \cdot n = \bar{t}$ on Γ_t, where $\bar{u}$ and $\bar{t}$ are prescribed displacements and tractions along the boundary Γ, and $\Gamma = \Gamma_u \cup \Gamma_t$. Aside from u, p is now an additional unknown that must be solved as part of the boundary value problem.

2.5 Weak form of the problem

To define the weak form of the problem, it is necessary to initially define the right spaces of the used functions which can solve the given problem. The $\mathcal{L}_2$ space ensures that the function is square integrable while the $\mathcal{H}^1$ spaces ensures that the first derivative of the function is square integrable.

$$\mathcal{L}_2 = \left\{ x \middle| \int_\Omega x^2 \, d\Omega < \infty \right\} \tag{33}$$

$$\mathcal{H}^1 = \{ x \in \mathcal{L}_2 \,\&\, x_{,i} \in \mathcal{L}_2 \} \tag{34}$$

Consider a problem domain Ω bounded by Γ, and weighting functions u^* and p^* that are both in $\mathcal{H}^1$ and satisfy the Dirichlet boundary conditions of the problem, the corresponding

weak form is given by

$$\int_\Omega 2\mu\varepsilon_d^* : \varepsilon_d \, d\Omega + \int_\Omega \varepsilon_v^* \cdot p \, d\Omega = \int_\Omega u^* \cdot f \, d\Omega + \int_\Gamma u^* \cdot t \, d\Gamma \tag{35}$$

The preceding equation is obtained from the equations of equilibrium in which the Cauchy stress tensor is decomposed into volumetric and deviatoric components, after which deviatoric term is expressed in terms of the deviatoric component of strains using Generalized Hooke's Law.

Next, combining the volumetric stress-strain relationship with the volumetric strain expressed in terms of the displacements, and the requirement of the Beltrami-Michell equations for the mean stress assuming constant body forces, and weighting by the function p^* gives

$$\int_\Omega p^* \varepsilon_v \, d\Omega - \int_\Omega \frac{1}{K} p^* p \, d\Omega + \int_\Omega \nabla p^* \cdot \nabla p \, d\Omega - \oint_\Gamma p^* \cdot q_n \, d\Gamma = 0 \tag{36}$$

where

$$\varepsilon_v^* = \nabla \cdot u^* \tag{37}$$

$$\varepsilon_d^* = A : \frac{1}{2} [\nabla u^* + (\nabla u^*)^T] \tag{38}$$

$$q = n \cdot \nabla p \tag{39}$$

2.6 Finite element model

Applying the weak form to the element domain Ω^e bounded by Γ^e, and subject to the following approximate interpolation

$$u(x) \approx \sum_{j=1}^N \psi_j(x) \hat{u}_j \tag{40}$$

$$p(x) \approx \sum_{j=1}^N \psi_j(x) \hat{p}_j \tag{41}$$

The resulting finite element model is given by the matrix equation

$$\begin{bmatrix} K^{uu} & K^{up} \\ K^{pu} & K^{pp} \end{bmatrix} \begin{Bmatrix} \hat{u} \\ \hat{p} \end{Bmatrix} = \begin{Bmatrix} f \\ 0 \end{Bmatrix} + \begin{Bmatrix} t \\ 0 \end{Bmatrix} \tag{42}$$

where

$$\{\hat{u}\} = \begin{Bmatrix} u_{1x} \\ u_{1y} \\ u_{2x} \\ u_{2y} \\ \vdots \\ u_{Nx} u_{Ny} \end{Bmatrix} \tag{43}$$

$$p \approx N \cdot \hat{p} \tag{44}$$

$$\nabla p \approx S \cdot \hat{p} \tag{45}$$

$$\{\hat{\boldsymbol{p}}\} = \begin{Bmatrix} p_1 \\ p_2 \\ \vdots \\ p_N \end{Bmatrix} \tag{46}$$

$$\{N\} = \{\psi_1 \quad \psi_2 \quad \cdots \quad \psi_N\} \tag{47}$$

$$[S] = \begin{bmatrix} \dfrac{\partial \psi_1}{\partial x} & \dfrac{\partial \psi_2}{\partial x} & \cdots & \dfrac{\partial \psi_N}{\partial x} \\ \dfrac{\partial \psi_1}{\partial y} & \dfrac{\partial \psi_2}{\partial y} & \cdots & \dfrac{\partial \psi_N}{\partial y} \end{bmatrix} \tag{48}$$

$$[Q] = \begin{bmatrix} n_x \dfrac{\partial \psi_1}{\partial x} + n_y \dfrac{\partial \psi_1}{\partial y} & n_x \dfrac{\partial \psi_2}{\partial x} + n_y \dfrac{\partial \psi_2}{\partial y} & \cdots & n_x \dfrac{\partial \psi_n}{\partial x} + n_y \dfrac{\partial \psi_n}{\partial y} \end{bmatrix} \tag{49}$$

$$[K_{ij}^{uu}] = \int_{\Omega^e} \underbrace{\tilde{B}_i^T \tilde{D} \tilde{B}_j}_{2\mu\varepsilon_d^*:\varepsilon_d} \, d\Omega^e \tag{50}$$

$$[K_{ij}^{up}] = \int_{\Omega^e} \underbrace{\bar{B}_i^T N_j}_{\varepsilon_v^* \cdot p} \, d\Omega^e \tag{51}$$

$$[K_{ij}^{pu}] = [K_{ij}^{up}]^T = \int_{\Omega^e} \underbrace{N_i^T \bar{B}_j}_{p^* \varepsilon_v} \, d\Omega^e \tag{52}$$

$$[K_{ij}^{pp}] = \int_{\Omega^e} \underbrace{S_i^T S_j}_{\nabla p^* \cdot \nabla p} \, d\Omega^e - \frac{1}{K} \int_{\Omega^e} \underbrace{N_i^T N_j}_{p^* p} \, d\Omega^e - \oint_{\Gamma^e} \underbrace{N_i^T Q_j}_{p^* \cdot q_n} d\Gamma^e \tag{53}$$

In this study, a stabilizing term is added to the vanishing part of the matrix $[K_{ij}^{pp}]$ in incompressible media so that the problem will not be ill-posed as can be seen in the previous equation. The rationale behind the stabilizing term used above is that for the pressure distribution to be smooth over a particular problem, the pressure values at the nodes of each element must be approximately equal within the element. Instead of using the shape functions,

the derivatives of the shape functions are used. Since the shape functions of the linear triangular element are linear, the derivatives would then have a constant value. This helps facilitate the constant pressure that should be obtained inside a particular element. Moreover, to ensure consistency with the deviatoric stresses and strains, a constant pressure field in the element must be enforced. To do this, the boundary term which corresponds to the fluxes across the element boundaries is set to zero, artificially forcing the pressure field to be constant within the element as the mesh is refined.

$$t = G \cdot \hat{t} \tag{54}$$

$$\hat{t} = \begin{Bmatrix} t_{1x} \\ t_{1y} \\ t_{2x} \\ t_{2y} \\ \vdots \\ t_{Nx} \\ t_{Ny} \end{Bmatrix} \tag{55}$$

$$\{t_i\} = \oint_{\Gamma^e} G_{ij} \hat{t}_j \, d\Gamma^e \tag{56}$$

$$f = G \cdot \hat{f} \tag{57}$$

$$\hat{f} = \begin{Bmatrix} f_x \\ f_y \end{Bmatrix} \tag{58}$$

$$\{f_i\} = \int_{\Omega^e} G_{ij} \hat{f}_j \, d\Omega^e \tag{59}$$

$$G = \begin{bmatrix} \psi_1 & 0 & \psi_2 & 0 & \cdots & \psi_N & 0 \\ 0 & \psi_1 & 0 & \psi_2 & \cdots & 0 & \psi_N \end{bmatrix} \tag{60}$$

The matrices $A, B, \widetilde{B}$, and $\widetilde{D}$ depend on the type of plane problem. The following must be initially defined before establishing the aforementioned matrices

$$\varepsilon = B \cdot \hat{u} \tag{61}$$

$$\varepsilon_v = \overline{B} \cdot \hat{u} \tag{62}$$

$$\varepsilon_d = \widetilde{B} \cdot \hat{u} \tag{63}$$

$$\widetilde{B} = A \cdot B \tag{64}$$

$$s = \widetilde{D} \cdot \varepsilon_d \tag{65}$$

$$\overline{B} = \frac{1}{3}\begin{bmatrix} \frac{\partial \psi_1}{\partial x} + \frac{\psi_1}{x} & \frac{\partial \psi_1}{\partial y} & \frac{\partial \psi_2}{\partial x} + \frac{\psi_2}{x} & \frac{\partial \psi_2}{\partial y} & \cdots & \frac{\partial \psi_N}{\partial x} + \frac{\psi_N}{x} & \frac{\partial \psi_N}{\partial y} \end{bmatrix} \tag{66}$$

For axisymmetric conditions

$$B = \begin{bmatrix} \frac{\partial \psi_1}{\partial x} & 0 & \frac{\partial \psi_2}{\partial x} & 0 & \cdots & \frac{\partial \psi_N}{\partial x} & 0 \\ 0 & \frac{\partial \psi_1}{\partial y} & 0 & \frac{\partial \psi_2}{\partial y} & \cdots & 0 & \frac{\partial \psi_N}{\partial y} \\ \frac{\partial \psi_1}{\partial y} & \frac{\partial \psi_1}{\partial x} & \frac{\partial \psi_2}{\partial y} & \frac{\partial \psi_2}{\partial x} & \cdots & \frac{\partial \psi_N}{\partial y} & \frac{\partial \psi_N}{\partial x} \\ \frac{\psi_1}{x} & 0 & \frac{\psi_2}{x} & 0 & \cdots & \frac{\psi_N}{x} & 0 \end{bmatrix} \tag{67}$$

$$A = \frac{1}{3}\begin{bmatrix} 2 & -1 & 0 & -1 \\ -1 & 2 & 0 & -1 \\ 0 & 0 & 1 & 0 \\ -1 & -1 & 0 & 2 \end{bmatrix} \tag{68}$$

$$\widetilde{D} = \begin{bmatrix} 2\mu & 0 & 0 & 0 \\ 0 & 2\mu & 0 & 0 \\ 0 & 0 & \mu & 0 \\ 0 & 0 & 0 & 2\mu \end{bmatrix} \tag{69}$$

For plane strain conditions

$$B = \begin{bmatrix} \frac{\partial \psi_1}{\partial x} & 0 & \frac{\partial \psi_2}{\partial x} & 0 & \cdots & \frac{\partial \psi_N}{\partial x} & 0 \\ 0 & \frac{\partial \psi_1}{\partial y} & 0 & \frac{\partial \psi_2}{\partial y} & \cdots & 0 & \frac{\partial \psi_N}{\partial y} \\ \frac{\partial \psi_1}{\partial y} & \frac{\partial \psi_1}{\partial x} & \frac{\partial \psi_2}{\partial y} & \frac{\partial \psi_2}{\partial x} & \cdots & \frac{\partial \psi_N}{\partial y} & \frac{\partial \psi_N}{\partial x} \end{bmatrix} \tag{70}$$

$$A = \frac{1}{3}\begin{bmatrix} 2 & -1 & 0 \\ -1 & 2 & 0 \\ 0 & 0 & 1 \end{bmatrix} \tag{71}$$

$$\widetilde{D} = \begin{bmatrix} 2\mu & 0 & 0 \\ 0 & 2\mu & 0 \\ 0 & 0 & \mu \end{bmatrix} \tag{72}$$

III. VERIFICATION OF STABILIZATION TECHNIQUE

Before presenting numerical examples, the stabilization technique used in the finite element analysis is verified to determine whether a significant reduction on the locking of the nodal displacements will be observed due to incompressibility of the element. By comparing the performance of the stabilized and unstabilized models, we can demonstrate the clear benefits of stabilization in preventing volumetric locking. This step sets the foundation for subsequent numerical examples, ensuring that our analyses are based on a robust and validated computational approach. The outcomes of this verification will underscore the necessity of stabilization techniques in accurately simulating the behavior of incompressible materials under various loading conditions.
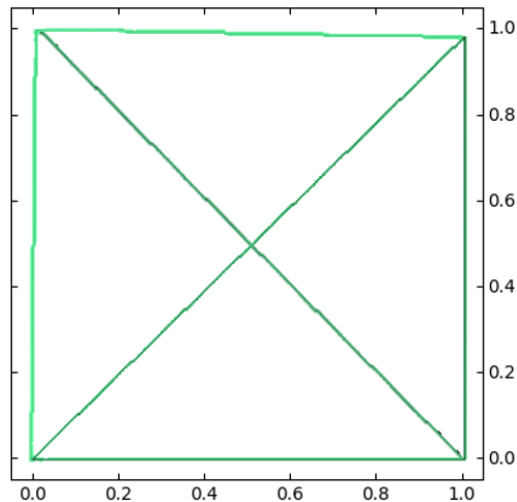
To verify the stabilization technique, a simple mesh and a simple problem was used, since the displacements obtained from an unstabilized analysis become more accurate as the mesh becomes finer. The nodes were also bounded in a way that would induce locking for the incompressible state in unstabilized analysis.

A representation of the problem is shown in Figure 1. It is made up of a unit square with a uniform vertical loading at the top and only four triangular elements. Since the model is designed to be an axisymmetric problem, the right side of the square acts as the axis of symmetry whereby all points on this line were bounded to move only along the vertical direction. The bottom surface was bounded to move only along the horizontal direction. The left surface was modeled as a free surface, such that all points in the line were free to displace in any direction. The top surface is where the load was applied. Also, all points on the top surface were restricted to move only in the vertical direction, so that its length was constant no matter the displacement that occurred. The uniform load applied has a magnitude of 5,000 kPa. For the incompressible medium, the modulus of elasticity was 10,000 kPa and the Poisson's ratio was given a value of 0.4999.
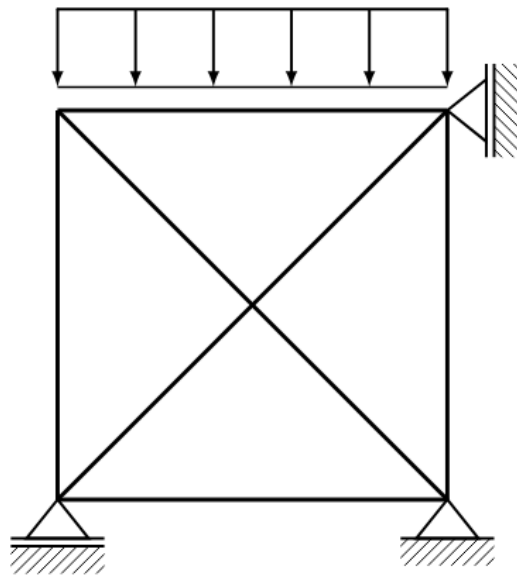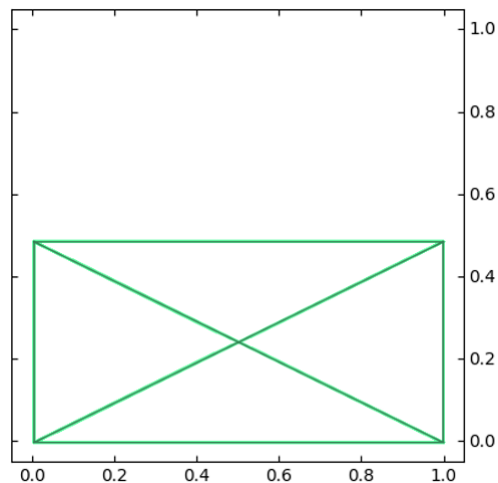

Figure 1. Set-up of verification problem

As can be seen in Figure 2, as expected, the results from the unstabilized analysis revealed significant locking issues. This was evidenced by the model's failure to deform appropriately under the applied load, with nodal displacements being severely restricted. The locking observed in the unstabilized model led to an overly stiff response, which did not accurately reflect the expected physical behavior of the model. Furthermore, the incompressibility of the material, characterized by a Poisson's ratio of 0.4999, made it worse since the problem became ill-posed.

Figure 2. Deformed configuration of verification problem (unstabilized method)

Upon applying the stabilization technique, a significant improvement was observed. The stabilized model demonstrated a significant reduction in locking, allowing for more realistic deformation under the same loading conditions as shown in Figure 3.

Figure 3. Deformed configuration of verification problem (stabilized method)

The following equations represent the analytical solution of the problem which simulates a simple triaxial test

$$\sigma = \begin{bmatrix} \sigma_{zz} & 0 & 0 \\ 0 & \sigma_{rr} & 0 \\ 0 & 0 & \sigma_{rr} \end{bmatrix} \tag{73}$$

$$s = \sigma - p1 = \begin{bmatrix} s_{zz} & 0 & 0 \\ 0 & s_{rr} & 0 \\ 0 & 0 & s_{rr} \end{bmatrix} = \begin{bmatrix} \sigma_{zz} - p & 0 & 0 \\ 0 & \sigma_{rr} - p & 0 \\ 0 & 0 & \sigma_{rr} - p \end{bmatrix} \tag{74}$$

$$\varepsilon_d = \frac{1}{2G}s = \frac{1}{2G}\begin{bmatrix} \sigma_{zz} - p & 0 & 0 \\ 0 & \sigma_{rr} - p & 0 \\ 0 & 0 & \sigma_{rr} - p \end{bmatrix} \tag{75}$$

Since the model is incompressible, $\varepsilon_v = 0$ such that

$$\varepsilon_d = \varepsilon - \varepsilon_v 1 = \varepsilon = \begin{bmatrix} \varepsilon_{zz} & 0 & 0 \\ 0 & \varepsilon_{rr} & 0 \\ 0 & 0 & \varepsilon_{rr} \end{bmatrix} = \begin{bmatrix} \varepsilon_{zz} & 0 & 0 \\ 0 & -\dfrac{\varepsilon_{zz}}{2} & 0 \\ 0 & 0 & -\dfrac{\varepsilon_{zz}}{2} \end{bmatrix} \tag{76}$$

$$\varepsilon_{zz} = \frac{\partial u_z}{\partial z} \tag{77}$$

$$u_z(z) = \left[\frac{\sigma_{zz} - p}{2G}\right]z \tag{78}$$

The analytical solution predicts a displacement of 0.5 m at the top of the model. In comparison, the stabilized finite element model with just four elements produces a displacement at the top of 0.49 m. With further mesh refinement, the computed displacement is expected to converge even more closely to the analytical solution, demonstrating improved accuracy. The displacements are now in line with theoretical expectations, indicating that the stabilization technique effectively addressed the numerical challenges posed by the incompressibility of the material.

This analysis confirms that the stabilization technique is essential for accurate finite element modeling of incompressible media. By preventing the locking of nodal displacements, the stabilization method ensures that the finite element analysis can reliably simulate the stress distribution and deformation behavior of a material.

IV. NUMERICAL EXAMPLE

This section will highlight the role of the proposed procedure in the finite element analysis of incompressible media within the context of geotechnical engineering problems particularly an axisymmetric problem involving an infinite half-space loaded by a circular area (circular footing). The example will illustrate the impact of the stabilization procedure on the pressure distribution and deformation patterns within the incompressible media.

Soils are porous materials with voids which can be filled with water, air, and other fluids. When a soil is saturated, the voids between soil particles are filled with water, and since water is nearly incompressible, the overall compressibility of the soil is reduced as well. Soil incompressibility results from situations when saturated soil deforms at a constant water content or void ratio wherein the soil does not experience any volume change. Upon loading, the stress cannot immediately dissipate as the water cannot easily escape the soil matrix, making the soil mass behave in an incompressible or almost incompressible manner. The build-up of excess pore water pressure in saturated soils makes it respond as an incompressible material until the water drains out and consolidation occurs. This is especially pronounced in low permeability soils like clays.

The insights gained from these simulations are crucial for advancing the design and analysis of foundations in geotechnical engineering, ensuring that structures built on such media are safe, stable, and efficient.
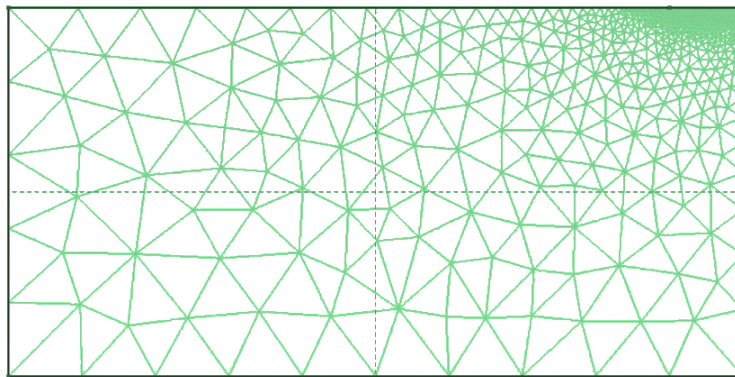
4.1 Axisymmetric footing problem

In this example, an axisymmetric problem is solved represented by a uniform circular load acting on the surface of an infinite half-space. Figure 4 shows a schematic representation of the configuration and dimensions used for the problem. The right face represents the axis of symmetry while the left face and the bottom represent a rigid wall and a rigid floor, respectively. The top surface is a free surface which was made significantly longer than the loaded surface for a better representation of an infinite half-space.
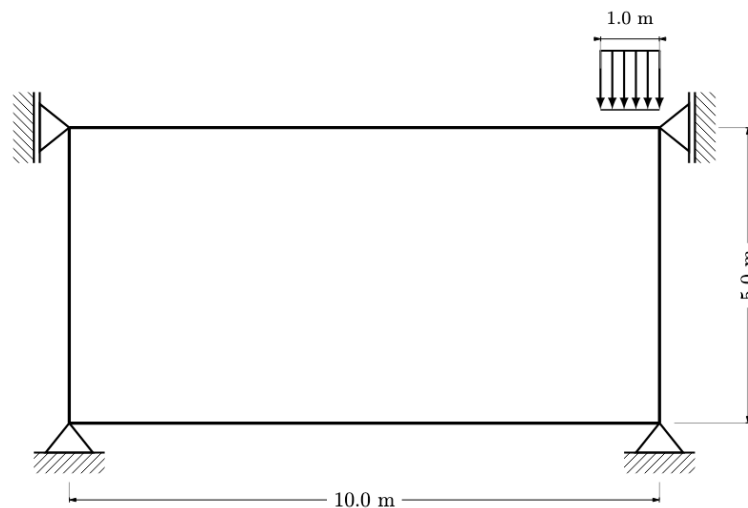
Figure 4. Set-up of axisymmetric footing problem

Since the bottom surface is a rigid floor, points on that line were only restricted to move in the radial direction, again resembling a roller in the horizontal direction. Points on both the left and right walls were restricted to move in the vertical direction. The top surface is a free surface and had no restrictions in movement.

The meshing for the problem was done to ensure accuracy and stability in the finite element analysis. We employed equal-order triangular elements, which offer flexibility in capturing complex geometries and stress variations. The mesh comprised 1364 nodes and 2498 unstructured triangular elements, strategically refined near the area where the load was applied as shown in Figure 5. An initial standard element size factor of 1 was applied uniformly across the system. However, to enhance the accuracy of results in the critical region near the load application, a finer mesh was required. Specifically, an element size factor of 0.007 was applied in this area to achieve improved computational accuracy. This finer mesh in the critical loading zone ensures that the stress gradients and deformation patterns are accurately resolved, capturing the intricate details of the soil's response under the circular footing. The gradual transition to a coarser mesh away from the loading area maintains computational efficiency without sacrificing the precision needed in the regions of interest. This meshing strategy balances accuracy and computational resources, providing a robust foundation for analyzing the stabilization techniques applied to the problem.


**Figure 5.** Meshing used for axisymmetric footing problem

In this study, the material properties of the soil were chosen to reflect the behavior of an incompressible medium under a footing load. The modulus of elasticity of the soil was set at 10,000 kPa, providing a measure of the soil's stiffness and its ability to deform elastically under stress. The Poisson's ratio was specified as 0.4999, which closely approximates the behavior of an incompressible material, indicating that the soil experiences minimal to no volume change under loading. The magnitude of the load applied was 5,000 kPa, representing the pressure exerted on the soil by the footing. These material properties were critical in simulating the stress distribution and deformation accurately, especially considering the near-incompressible nature of the soil and ensuring that the stabilization techniques could be effectively evaluated in this context.

As earlier established in the verification problem, for the unstabilized analysis, locking was observed, leading to an overly stiff response and unrealistic displacement patterns. However, for this footing problem, we can see from Figure 6 and Figure 7, that as the mesh was further refined and the number of elements increased, the displacements became more accurate even for the unstabilized analysis. This improvement was attributed to the elements being less restricted by the boundary conditions and able to deform more naturally without changing their respective areas. In finer meshes, the elements had higher resolution and better flexibility to accommodate the stress distribution, which mitigated some of the locking effects inherent in the unstabilized method. It is evident that while the unstabilized method can achieve accuracy in terms of displacement with extremely fine meshes, it is computationally inefficient and still prone to locking with coarser meshes.
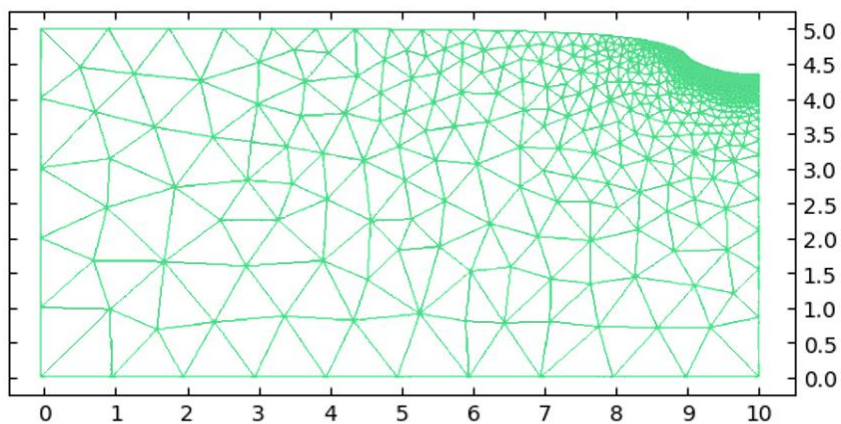

Figure 6. Deformed configuration of footing problem (unstabilized method)
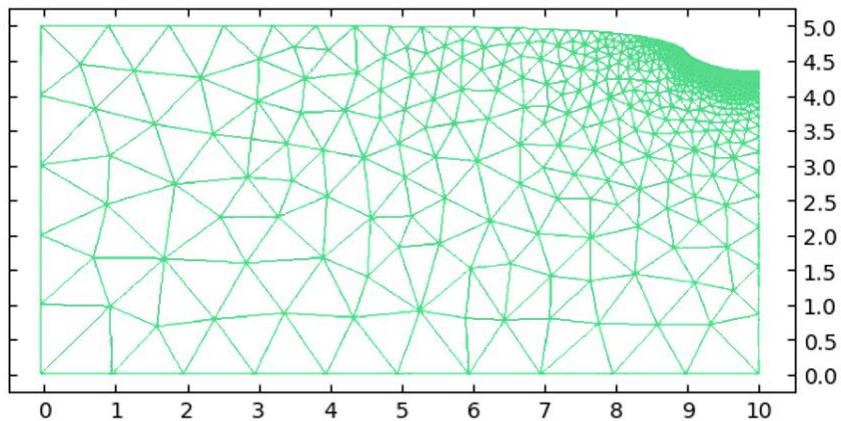
Figure 7. Deformed configuration of footing problem (stabilized method)

As equally important, in addition to displacement comparisons, the pressure distribution within the soil was analyzed for both unstabilized and stabilized methods. For the unstabilized method, the pressure distribution exhibited considerable oscillations in the system as illustrated in Figure 8. Spurious pressures as low as -1970 kPa and as high as 6810 kPa were also observed in the system. These oscillations indicated numerical instabilities in capturing the states of stress within the soil. The pressure field was not smooth, with abrupt changes reflecting the

inadequacy of the unstabilized method in handling the incompressibility of the material. This erratic pressure distribution can lead to incorrect predictions of soil behavior and potential design flaws in practical engineering applications.
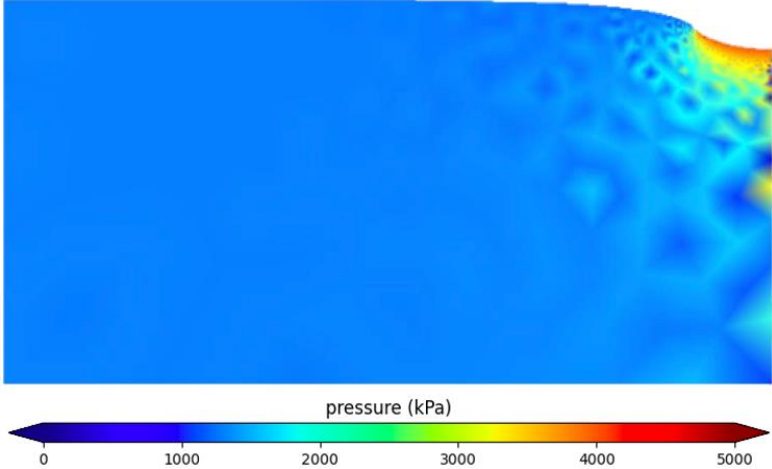

Figure 8. Footing problem pressure distribution (unstabilized method)

In contrast, the stabilized method produced a much smoother and more realistic pressure distribution. The stabilization technique effectively mitigated the oscillations observed in the unstabilized method, resulting in a pressure field that accurately reflected the expected stress patterns under the applied load as can be seen in Figure 9. It can be noticed that the map of the pressure smoothly transitions from one end of the color spectrum to the other as it moves away from the surface of application of the load. This demonstrates the capability of the stabilized method to handle the complexities of incompressible materials.
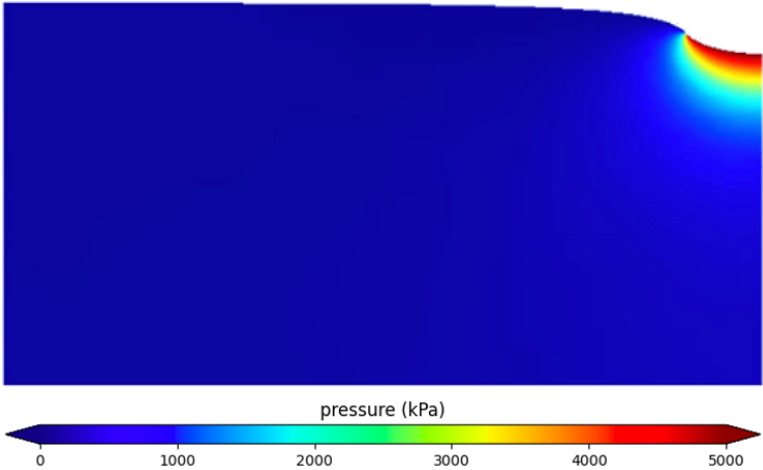
Figure 9. Footing problem pressure distribution (stabilized method)

Figure 10 which illustrates the continuity and smoothness of the pressure field across elements via filled iso-values also show that the formulation and stabilization technique applied is successful in obtaining constant pressures which is expected within each element. The pressure fields do not exhibit a "checkerboard" pattern that is typical in unstabilized cases, and is hence, free from the locking phenomena. Also, the iso-values are uniformly filled without any discontinuities. The absence of gaps or abrupt jumps between the colors representing different pressure levels demonstrates the pressure solution at the nodes of each element has been accurately interpolated and stabilized.
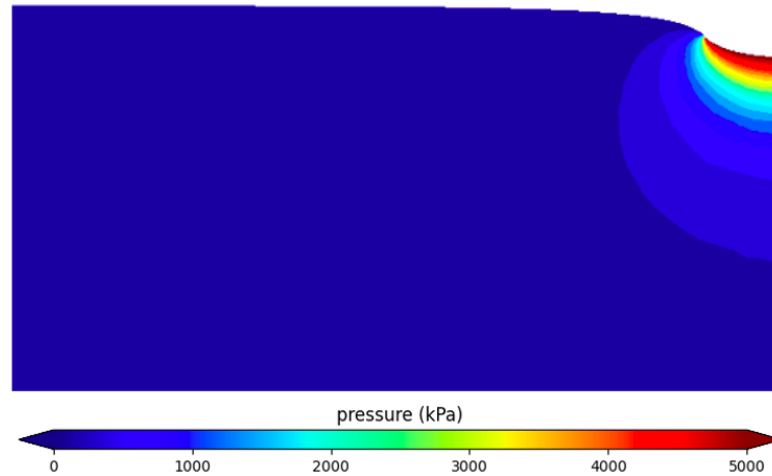
Figure 10. Filled iso-values of the pressure field (stabilized method)

To further validate the stabilization technique used, the results of the stabilized method are compared with the well-established Boussinesq solution [25,26]. The comparison focuses on the pressure distributions both at the surface of the domain and along the axis of symmetry.

For the surface pressures, the pressure values were plotted against the radial distance from the center of the load as shown in Figure 11. At the surface, from the Boussinesq solution, the pressure obtained was 5,000 kPa within the load, 2,500 kPa at the edge of the load, and 0 kPa outside the load. Notice a sudden drop in pressure at the edge of the load. The drop is steeper in the Boussinesq solution, while the transition in pressure values in the stabilized finite element method was more gradual.
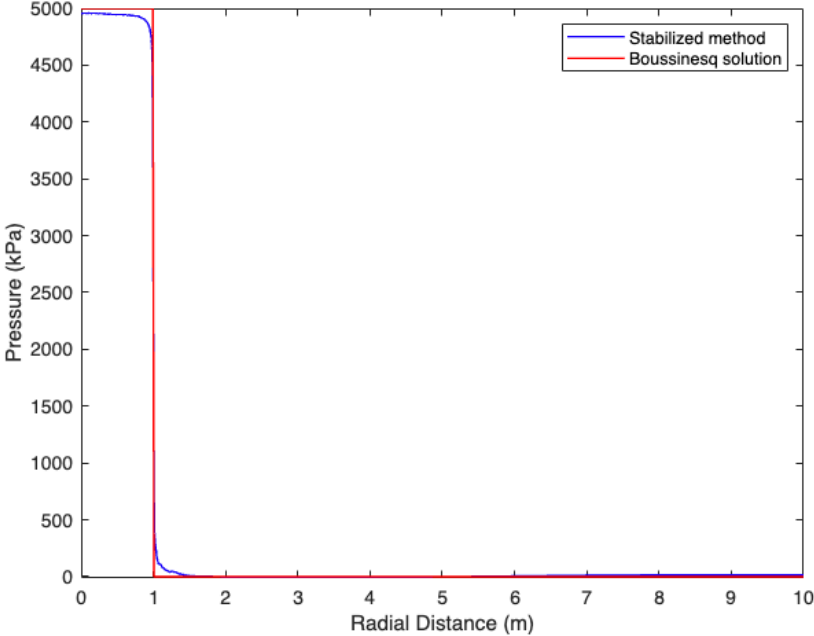
Figure 11. Comparison of pressures at the surface with respect to radial distance

Similarly, for pressures generated along the axis of symmetry, the pressure values were plotted against the depth from the surface as shown in Figure 12. The Boussinesq solution provides a clear expectation for how pressure varies with depth, typically showing a decrease in pressure as depth increases. The results from the stabilized finite element method closely matched the analytical solution, demonstrating that the pressure distribution along the axis of symmetry was accurately captured.
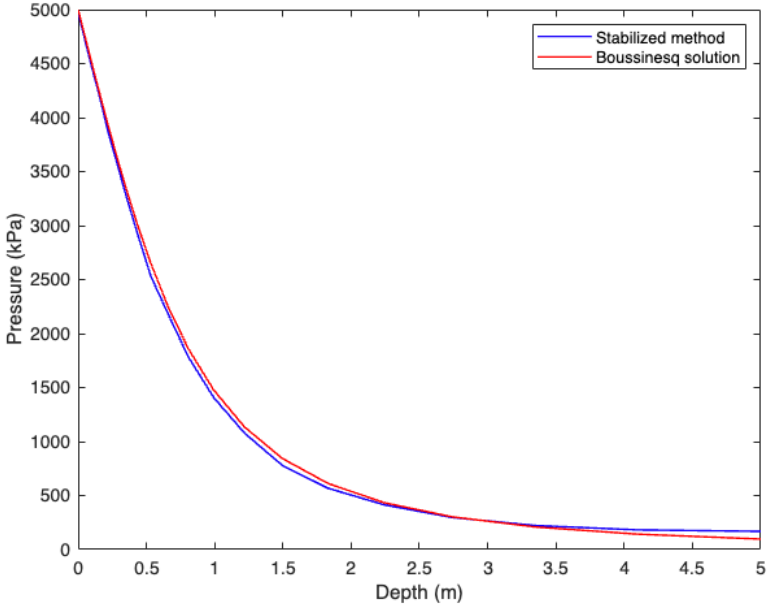

Figure 12. Comparison of pressures at the axis of symmetry with respect to depth

The comparison between the stabilized finite element method and the Boussinesq solution shows that the stabilized method produces results that are in strong agreement with the well-established theoretical expectations.

V. CONCLUSION

This study has successfully shown how a modified mixed formulation of the finite element method with stabilization using equal-order triangular elements can be used to accurately model and capture the behavior of incompressible media. By using an approach that incorporates both displacements and pressures as degrees of freedom, the formulation addresses the inherent challenges and limitations of traditional displacement-based methods to solve such problems.

The modified mixed formulation with stabilization developed in this study also effectively circumvents the issue of locking as the media approaches incompressibility. The following are the key features of the modified mixed formulation: the decomposition of stresses and strains into deviatoric and volumetric components to make them uncoupled, the use of bulk modulus K instead of the Lam*é* parameter λ in the constitutive equations, and the imposition of the Beltrami-Michell compatibility equations.

Another critical component of the study was the addition of a stabilizing term to the formulation. This term prevents the problem from becoming ill-posed, which is a common issue in the finite element analysis of incompressible media. As shown through the numerical examples, the stabilizing term produced results that are comparable to known analytical solutions and was able to provide accurate stress distributions and deformation behaviors. Furthermore, instead of relying on the shape functions themselves in the stabilizing term, the study utilized the derivatives of these functions. Given that the shape functions for linear triangular elements are linear, their derivatives are constant. This approach simplifies the computation and ensures that the pressure within each element remains constant, aligning with the physical expectation for incompressible media.

Despite the simplicity of lower order triangular elements, the study has shown that these elements remain valuable due to their computational efficiency and ease of implementation. When combined with the proposed formulation and stabilization technique, lower order triangular elements provide accurate results even for incompressible media, which are traditionally challenging to model.

References:
[1]   Reddy JN. 2019. Introduction to the finite element method. 4th ed. New York: McGraw-Hill Education
[2]   Srinivasan R, Perucchio R. 1994. Finite element analysis of anisotropic non-linear incompressible
[3]   elastic solids by a mixed model. International Journal for Numerical Methods in Engineering. 37(18): 3075-3092.
[4]   Hughes TJ. 1980. Generalization of selective integration procedures to anisotropic and nonlinear media. International Journal for Numerical Methods in Engineering. 15(9):1413-1418.
[5]   Bathe KJ. 2006. Finite element procedures. Klaus-Jurgen Bathe.

[6]   Babuska I. 1971. Error-bounds for finite element method. Numerische Mathematik. 16(4):322-33.

[7]   Brezzi F. 1974. On the existence, uniqueness and approximation of saddle-point problems arising from lagrangian multipliers. Publications des sémainaires de mathématiques et informatique de Renne. S4: 1-26.

[8]   Preisig M, Prevost J. 2013. New findings on limit state analysis with unstructured triangular finite elements. International Journal for Numerical Methods in Engineering. 94(4):400-417.

[9]   Brezzi F, Pitkaranta J. 1984. On the stabilization of finite element approximations of the stokes equations. Efficient Solutions of Elliptic Systems: Proceedings of a GAMM-Seminar Kiel. p. 11-19.

[10]   Hughes TJ, Franca LP, Balestra M. 1986. A new finite element formulation for computational fluid dynamics: V. circumventing the babuška-brezzi condition: A stable petrov-galerkin formulation of the stokes problem accommodating equal-order interpolations. Computer Methods in Applied Mechanics and Engineering. 59(1):85-99.

[11]   Barth T, Bochev P, Gunzburger M, Shadid J. 2004. A taxonomy of consistently stabilized finite element methods for the stokes problem. SIAM Journal on Scientific Computing. 25(5):85-1607.

[12]   Brezzi F, Fortin M. 2012. Mixed and hybrid finite element methods. Vol. 15. Springer Science & Business Media.

[13]   Chen JS, Pan C, Chang TYP. 1995. On the control of pressure oscillation in bilinear-displacement constant-pressure element. Computer methods in applied mechanics and engineering. 128(1-2):137-152.

[14]   Fortin M. 1981. Old and new finite elements for incompressible flows. International Journal for Numerical Methods in Fluids. 1(4):347-364.

[15]   Sani RL, Gresho PM, Lee RL, Griffiths DF. 1981. The cause and cure (?) of the spurious pressures generated by certain FEM solutions of the incompressible Navier-Stokes equations: Part 1. International Journal for Numerical Methods in Fluids. 1(1):17-43.

[16]   Nagtegaal JC, Parks DM, Rice J. 1974. On numerically accurate finite element solutions in the fully plastic range. Computer Methods in Applied Mechanics and Engineering. 4(2):153-177.

[17]   Oden, JT, Key JE. 1970. Numerical analysis of finite axisymmetric deformations of incompressible elastic solids of revolution. International Journal of Solids and Structures. 6(5):497-518.

[18]   Key SW. 1969. A variational principle for incompressible and nearly-incompressible anisotropic elasticity. International Journal of Solids and Structures. 5(9):951-964.

[19]   Hughes TJ. 2012. The finite element method: Linear static and dynamic finite element analysis. Courier Corporation.

[20]   Herrmann LR. 1965. Elasticity equations for incompressible and nearly incompressible materials by a variational theorem. AIAA Journal. 3(10):1896-1900.

[21]   Sussman T, Bathe KJ. 1987. A finite element formulation for nonlinear incompressible elastic and inelastic analysis. Computers & Structures. 26(1-2):357-409.

[22]   Beltrami E. 1892. Osservazioni sulla nota precedente. Atti Accad. Lincei Rend. 1(5):141-142.

[23]   Michell J. 1899. On the direct determination of stress in an elastic solid, with application to the theory of plates. Proceedings of the London Mathematical Society. 1(1):100-124.

[24]   Fung YC, Tong P, ChenX. 2001. Classical and computational solid mechanics. World Scientific.

[25]   Reddy JN. 2013. An introduction to continuum mechanics. Cambridge University Press.

[26]   Poulos HG, Davis EH. 1974. Elastic solutions for soil and rock mechanics. Centre for Geotechnical Research. University of Sydney.

[27]   Davis RO, Selvadurai AP. 2005. Plasticity and geomechanics. Cambridge University Press.